



# Impact of nonlinearity including bleaching in MUTC photodetectors on RF-modulated electro-optic frequency combs

SEYED EHSAN JAMALI MAHABADI,<sup>1,\*</sup>  THOMAS F. CARRUTHERS,<sup>1</sup>  CURTIS R. MENYUK,<sup>1</sup>  JASON D. MCKINNEY,<sup>2</sup> AND KEITH J. WILLIAMS<sup>2</sup>

<sup>1</sup>Department of Computer Science and Electrical Engineering, University of Maryland, Baltimore County, Baltimore, MD 21250, USA

<sup>2</sup>U.S. Naval Research Laboratory, Washington, DC 20375, USA

\*[sjamali1@umbc.edu](mailto:sjamali1@umbc.edu)

<http://www.photonics.umbc.edu>

**Abstract:** We use the drift-diffusion equations to calculate the responsivity of a modified uni-traveling carrier (MUTC) photodetector (PD) with a frequency comb input that is generated by a series of short optical pulses. We first use experimental results for the responsivity of the MUTC PD to obtain an empirical model of bleaching in pulsed mode. We incorporate our empirical bleaching model into a drift-diffusion model to calculate the impact of nonlinearity in an MUTC PD on RF-modulated electro-optic frequency combs. We quantify the nonlinearity using the second- and third-order intermodulation distortion powers (IMD2 and IMD3), from which we calculate the second- and third-order output intercept points (OIP2 and OIP3). In contrast to a continuous wave (CW) input for which there is a single IMD2 and IMD3 and hence a single OIP2 and OIP3, each comb line  $n$  has its own IMD<sub>2 $n$</sub> , IMD<sub>3 $n$</sub> , OIP<sub>2 $n$</sub> , and OIP<sub>3 $n$</sub>  associated with it. We determine the IMD<sub>2 $n$</sub> , IMD<sub>3 $n$</sub> , OIP<sub>2 $n$</sub> , and OIP<sub>3 $n$</sub> , and we compare the results with and without bleaching. We find that the impact of bleaching is complex and, somewhat surprisingly, not always detrimental. The principal effect of bleaching is to lower the responsivity, which decreases the nonlinearity due to space charge. While bleaching always reduces the OIP<sub>2 $n$</sub>  and OIP<sub>3 $n$</sub> , we find that bleaching leads to a decreased distortion-to-signal ratio for large  $n$ .

© 2021 Optical Society of America under the terms of the [OSA Open Access Publishing Agreement](#)

## 1. Introduction

In this paper, we study the impact of nonlinearity in a modified uni-traveling carrier (MUTC) photodetector (PD) on radio-frequency (RF) modulated frequency combs. This work describes in detail the impact of nonlinear saturation (bleaching) on an MUTC PD for the first time. We have done similar work for a  $p-i-n$  PD and that work was briefly summarized in [1] and will be discussed in more detail in a subsequent paper. Here, we expand prior work [2,3], and we elucidate the physics behind our prior results. In earlier work, we compared the impact of nonlinearity on  $p-i-n$  and MUTC PDs [4], but we did not elucidate the effect of bleaching.

Frequency combs play an important role in RF-photonics systems [5]. They provide the lowest close-in RF phase noise to date [6], increase the Brillouin threshold for transmission through optical fibers [7], and can be used to disambiguate radar signals [8]. Frequency combs can be generated in the optical domain by creating a stream of short pulses, using for example a short pulse laser [9] or a continuous wave laser followed by an electro-optic modulator [10]. These pulses may then be modulated by an RF signal. When the signal passes through a PD, an RF comb is produced in which the original RF modulation appears as sidebands around each comb

line. The pulses in a typical optical pulse train have durations less than 500 fs and are spaced by 10–50 ns. Hence, the peak-to-average power ratio is  $10^4$ – $10^5$  [2,3].

Bleaching or absorption saturation in a high-current PD can occur when intense optical fields deplete the number of available final energy states or depopulate the initial states [11]. Additionally, the high density of electrons that is created can increase the possibility that they are recaptured. Regardless of its origin, bleaching leads to a reduction in the PD's responsivity as the peak intensity and hence the average power increases. This reduction in responsivity can lead to nonlinear distortion of an incoming RF-photon signal. Juodawlkis *et al.* [11] have reported that this effect can limit the performance of photonic analog-to-digital converters (PADCs).

We developed an empirical model of bleaching and incorporated this model into a one-dimensional (1-D) drift-diffusion model that Hu *et al.* [12] previously developed. The bleaching model was based on experimental data that was collected at the Naval Research Laboratory (NRL). We then used this model to calculate the PD nonlinearity [1–4].

With a modulated CW input, the device nonlinearity can be characterized using the second- and third-order intermodulation distortion powers (IMD2 and IMD3 powers) and by the second- and third-order output intercept points (OIP2 and OIP3). This simple characterization is no longer possible when working with frequency combs since every electrical comb line is impacted by the nonlinearity in a different way. Instead, we define an  $IMD_{2,n}$ ,  $IMD_{3,n}$ ,  $OIP_{2,n}$ , and  $OIP_{3,n}$  for each comb line  $n$  [4].

We have found that the impact of bleaching on the nonlinear distortion products is complex and can somewhat surprisingly lead to lower values of the ratio of these products to the fundamental power at high  $n$ -values. Bleaching lowers the responsivity and thus decreases space charge effects that contribute to nonlinear distortion.

The remainder of this paper is organized as follows: In Sec. 2, we review the MUTC structure that we are using for our studies. In Sec. 3, we review our model of bleaching. In Sec. 4, we define the IMD2, IMD3, OIP2, and OIP3 for electro-optic frequency combs. In Sec. 5, we present our results for the MUTC structure.

## 2. MUTC structure

Figure 1 shows the MUTC PD structure [13] that we use in our model. Green indicates the absorption region, red indicates highly doped InP layers, purple indicates highly-doped InGaAs layers, and white indicates other layers. In each layer, we indicate the material, doping concentration, and thickness. In InGaAsP layers, Q1.1 and Q1.4 stand for quaternary compounds with bandgap wavelengths equal to 1.1  $\mu\text{m}$  and 1.4  $\mu\text{m}$ , respectively. We use  $n$  to indicate  $n$ -type doping,  $n^+$  to indicate a high  $n$ -type doping concentration,  $p$  to indicate  $p$ -type doping, and  $p^+$  to indicate a high  $p$ -type doping concentration.

## 3. Bleaching model

We developed our model of bleaching, starting from the well-known equations for emission and absorption for a two-level system [14]. We let  $N_1$  equal the population of the lower level,  $N_2$  equal the population of the upper level, and  $N = N_1 + N_2$  equal the total population. We then find that

$$\frac{N_1}{N} = \frac{A + BI_p}{C + DI_p}, \quad (1)$$

where  $I_p$  is the input optical power,  $B$  is the cross-section for stimulated absorption,  $D$  is the combined cross-section for stimulated absorption and emission, and  $A = C$  is proportional to the rate of spontaneous emission. We assume that  $N_1$  is the fraction of molecules that is available to create electron-hole pairs, and we multiply the generation rate in our drift-diffusion model by the factor  $\beta = N_1/N$ . The optical generation rate that we use in our drift-diffusion model  $G_{\text{opt}}$  is

|          |  |         |
|----------|--|---------|
| p-region | InGaAs, $p^+$ , Zn, $2.0 \times 10^{19}$ , 50 nm       | 50 nm   |
|          | InP, $p^+$ , Zn, $1.5 \times 10^{18}$ , 100 nm         | 150 nm  |
|          | InGaAsP, Q1.1, Zn, $2.0 \times 10^{18}$ , 15 nm        | 165 nm  |
|          | InGaAsP, Q1.4, Zn, $2.0 \times 10^{18}$ , 15 nm        | 180 nm  |
|          | InGaAs, $p$ , Zn, $2.0 \times 10^{18}$ , 100 nm        | 280 nm  |
|          | InGaAs, $p$ , Zn, $1.2 \times 10^{18}$ , 150 nm        | 430 nm  |
|          | InGaAs, $p$ , Zn, $8.0 \times 10^{17}$ , 200 nm        | 630 nm  |
|          | InGaAs, $p$ , Zn, $5.0 \times 10^{17}$ , 250 nm        | 880 nm  |
|          | InGaAs, Si, $1.0 \times 10^{16}$ , 150 nm              | 1030 nm |
| i-region | InGaAsP, Q1.4, Si, $1.0 \times 10^{16}$ , 15 nm        | 1045 nm |
|          | InGaAsP, Q1.1, Si, $1.0 \times 10^{16}$ , 15 nm        | 1060 nm |
|          | InP, Si, $1.4 \times 10^{17}$ , 50 nm                  | 1110 nm |
|          | InP, Si, $1.0 \times 10^{16}$ , 900 nm                 | 2010 nm |
| n-region | InP, $n^+$ , Si, $1.0 \times 10^{18}$ , 100 nm         | 2110 nm |
|          | InP, $n^+$ , Si, $1.0 \times 10^{19}$ , 900 nm         | 3010 nm |
|          | InGaAs, $n^+$ , Si, $1.0 \times 10^{19}$ , 20 nm       | 3030 nm |
|          | InP, $n^+$ , Si, $1.0 \times 10^{19}$ , 200 nm         | 3230 nm |
|          | InP, semi-insulating substrate<br>Double side polished |         |

**Fig. 1.** MUTC PD structure [13]. Green indicates the absorption regions, which include an intrinsic region and a  $p$ -doped region. Red indicates highly-doped InP layers, purple indicates highly-doped InGaAs layers, and white indicates other layers. This figure is the same as Fig. 1 in Hu *et al.*[12].

given by

$$G_{\text{opt}} = \beta G_c \exp[-\alpha(L - x)], \quad (2)$$

where  $G_c$  is the generation coefficient without bleaching,  $\alpha$  is the absorption coefficient,  $x$  is the distance across the device, and  $L$  is the device length. This model effectively assumes that the bleaching is instantaneous. That will not be the case in practice, but the finite response time will not affect the model as long as the time for the PD to return to the unbleached state is short compared to the repetition time.

In practice, the physics of bleaching is complex and poorly understood. In order to match the experimentally measured bleaching, it is necessary to modify our model so that  $A \neq B$ . Additionally, we found that in order to obtain all positive coefficients in the bleaching model from a least-squares fit to the data, we had to add a quadratic term to our model, which then becomes

$$\frac{N_1}{N} = \frac{A + BI_p}{C + DI_p + EI_p^2}. \quad (3)$$

Figure 2 shows experimental results of the responsivity of the MUTC PD as a function of the average input optical power with a pulsed input in which pulses have a FWHM duration of 100 fs and a repetition frequency of 50 MHz. The experimental data that we show in Fig. 2 are unpublished data that were collected at the Naval Research Laboratory. In the experiments, a Calmar Mendecino passively-modelocked erbium-doped fiber laser was used. The output of the modelocked laser was a train of pulses with a 100-fs FWHM pulse duration and a 50-MHz repetition rate. The output was passed through a variable attenuator and a calibrated optical tap

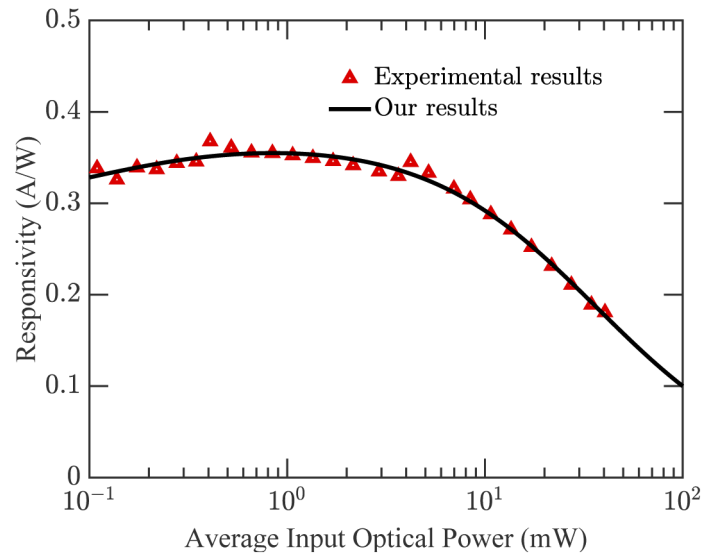


**Fig. 2.** Responsivity as a function of average power for the MUTC PD.

**Table 1. Empirical fitting parameters in Eq. (3) for the MUTC PD with a pulsed input.**

| Fitting parameters | MUTC   |
|--------------------|--------|
| $A$                | 1.0000 |
| $B$                | 0.0322 |
| $C$                | 2.7181 |
| $D$                | 0.1632 |
| $E$                | 0.0016 |

with a 90/10 splitter. The 10% tap was used as a power monitor and the 90% tap illuminated the MUTC PD. The average optical power and average photocurrent were measured as the optical attenuator was adjusted. Knowing the repetition rate, the optical power was then converted to a pulse energy to calculate the responsivity. We also show our empirical fit to this data [2,3] for the MUTC PD in pulsed mode using Eq. (3) and setting  $A = 1$ . Table 1 shows the values of  $A$ ,  $B$ ,  $C$ ,  $D$ , and  $E$  in Eq. (3). The simulations were performed with a 4-V bias, and the 3-dB bandwidth of the MUTC PD is 19 GHz, which is calculated using the impulse response of the MUTC PD [15].

#### 4. Nonlinearity characterization

We calculate the impact of bleaching on the device nonlinearity as a function of the average input optical power. When considering nonlinearity in PDs, IMD2 and IMD3 are particularly significant, since the frequencies that they generate can be close to the fundamental frequency and its harmonic frequencies in the case of IMD2 and also close to the fundamental modulation frequencies in the case of IMD3. The OIP2 and OIP3 are the key figures of merit to characterize the IMD2 and IMD3. The OIP2 and OIP3 are defined as the extrapolated intercept points of the power of the fundamental frequency and the IMD2 and IMD3 powers, respectively. Hence, they characterize the power ratio of the intermodulation products and the fundamental signal. On a log-log plot, the slope of the fundamental power is 1, and the slope of the IMD2 power is 2. The

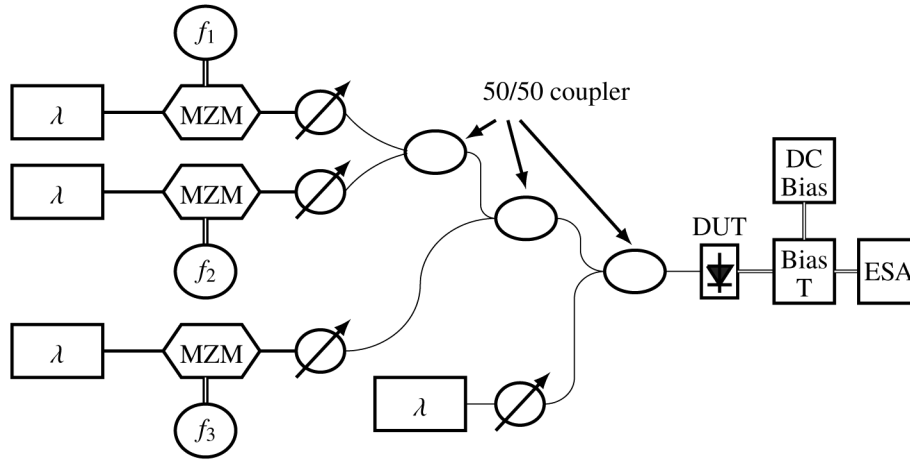


**Fig. 3.** A four-laser three-tone MZM measurement setup. This figure is similar to Fig. 2 in Draa *et al.* [18].

OIP2 can be calculated from the fundamental power and the IMD2 power; it is given in dBm by

$$\text{OIP2} = 2P_f - P_{\text{IMD2}}, \quad (4)$$

where  $P_f$  is the fundamental power in dBm and  $P_{\text{IMD2}}$  is the IMD2 power in dBm [16–18]. The slope of the IMD3 power on a log-log plot is 3. The OIP3 can be calculated from the fundamental power and the IMD3 power; it is given in dBm by

$$\text{OIP3} = P_f + \frac{1}{2} (P_f - P_{\text{IMD3}}), \quad (5)$$

where  $P_{\text{IMD3}}$  is the IMD3 power in dBm [16–19].

PD nonlinearity can be measured using one-, two-, and three-tone measurement systems [18]. Figure 3 shows the setup of a three-tone measurement system. Three Nd:YAG lasers operating at the same wavelength with the same pulse duration are modulated by three Mach-Zehnder modulators (MZMs) and their output is fed through optical attenuators. The first two modulated light frequencies are combined using a 50/50 coupler and are then combined with the third frequency using another 50/50 coupler. The unmodulated laser frequency is transmitted through a variable optical attenuator and is then combined with the signal using a final 50/50 coupler. The output is fed into the device under test (DUT). The RF output power is measured with an electrical spectrum analyzer (ESA). The modulation depth is varied by attenuating the lasers.

The input modulated light power  $P(t)$  of the optical envelope in a three-tone measurement system may be expressed as

$$P(t) = P_{\text{opt}}(t) \{1 + m [\sin(2\pi f_1 t) + \sin(2\pi f_2 t) + \sin(2\pi f_3 t)]\}, \quad (6)$$

where  $m$  is modulation depth,  $f_1$ ,  $f_2$ , and  $f_3$  are the three modulation frequencies, and  $P_{\text{opt}}(t)$  is the input light power of the optical envelope as a function of time. It is given by

$$P_{\text{opt}}(t) = \sum_n A \operatorname{sech}\left(\frac{t - nT_r}{\tau}\right), \quad (7)$$

where  $T_r$  is the repetition time and  $\tau$  is the pulse duration.

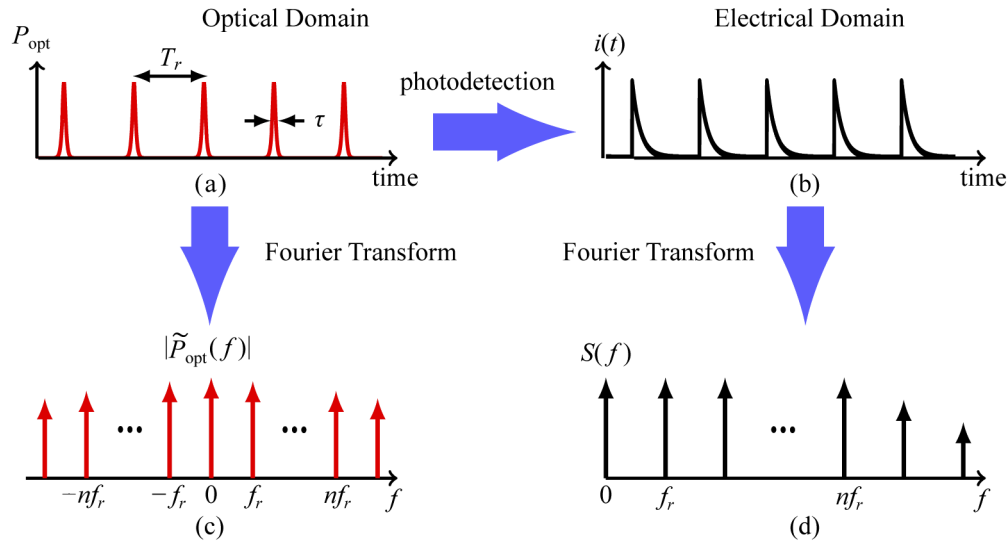


**Fig. 4.** Time and frequency domain depictions of the input optical and output electrical pulse trains, where  $T_r$  is the repetition time and  $\tau$  is the pulse duration of the optical signal. (a) Input optical pulse train intensity profile. (b) Output electrical pulse train. (c) Spectrum of the optical intensity profile. (d) Power spectrum of the photocurrent. This figure is similar to Fig. 1 in Quinlan *et al.*[20].

If we write the electric field as

$$\mathbf{E}(t) = \mathbf{E}_i(t) \exp(2\pi j f_0 t) + \mathbf{E}_i^*(t) \exp(-2\pi j f_0 t), \quad (8)$$

then we find that

$$P_{\text{opt}}(t) = 2A_{\text{eff}}\epsilon c |\mathbf{E}_i(t)|^2, \quad (9)$$

where  $A_{\text{eff}}$  is the effective area of the optical beam,  $\epsilon$  is the permeability, and  $c$  is the speed of light. The three frequencies should be close to each other. In our calculations, we used  $f_1 = 10$  MHz,  $f_2 = 10.5$  MHz, and  $f_3 = 9$  MHz. We chose these three frequencies so that they are close to each other, fall within the 50-MHz repetition frequency, and do not lead to aliasing. We use a total time window that is 2- $\mu$ s long and contains an integral number of periods for all three modulation frequencies, so that we avoid aliasing.

The use of frequency combs changes the characterization of nonlinearity in a fundamental way from its characterization for a modulated CW input. The IMD2 and IMD3 and hence the OIP2 and OIP3 all become functions of the comb line number  $n$  [4]. Figure 4 schematically illustrates the photodetection of a periodic train of optical pulses, which then produces a train of electrical pulses where  $\tilde{P}_{\text{opt}}(f)$  is the Fourier transform of  $P_{\text{opt}}(t)$  and  $S(f)$  is the power spectral density of the photocurrent. The periodic train of optical pulses corresponds to equally spaced comb lines in the frequency domain that are spaced by the repetition frequency and centered around zero [20]. The output of the PD is a periodic train of electrical pulses that corresponds to comb lines in the frequency domain that are again separated by the repetition frequency. We modulate the input optical pulses with the three frequencies  $f_1$ ,  $f_2$ , and  $f_3$  defined in Eq. (6).

Figure 5 shows time and frequency domain depictions of the modulated input optical pulse train and the output electrical pulse train after the PD, while Fig. 6 shows the spectrum of the modulated optical intensity profile and the corresponding frequency domain comb lines. The  $n$ -th comb line, which is shown by a red arrow, is surrounded by smaller lines at the modulated frequencies  $nf_r \pm f_1$ ,  $nf_r \pm f_2$ , and  $nf_r \pm f_3$ , which are shown by blue arrows. In the expanded view,

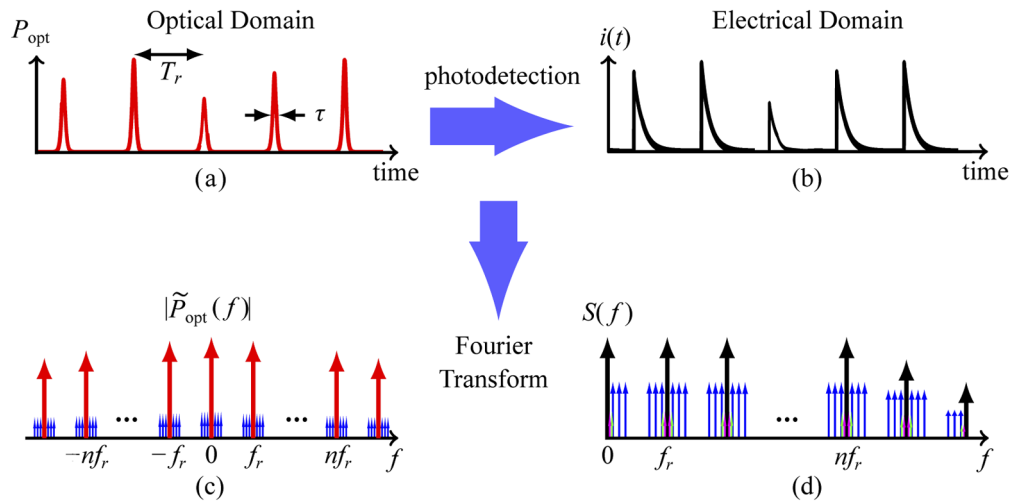


**Fig. 5.** Time and frequency domain depictions of modulated input optical and output electrical pulse trains, where  $T_r$  is the repetition time and  $\tau$  is the pulse duration of the optical signal. (a) Modulated input optical pulse train. (b) Modulated output electrical pulse train. (c) Spectrum of the modulated optical intensity. (d) Power spectrum of the modulated photocurrent. This figure is similar to Fig. 2 in Jamali *et al.*[4].

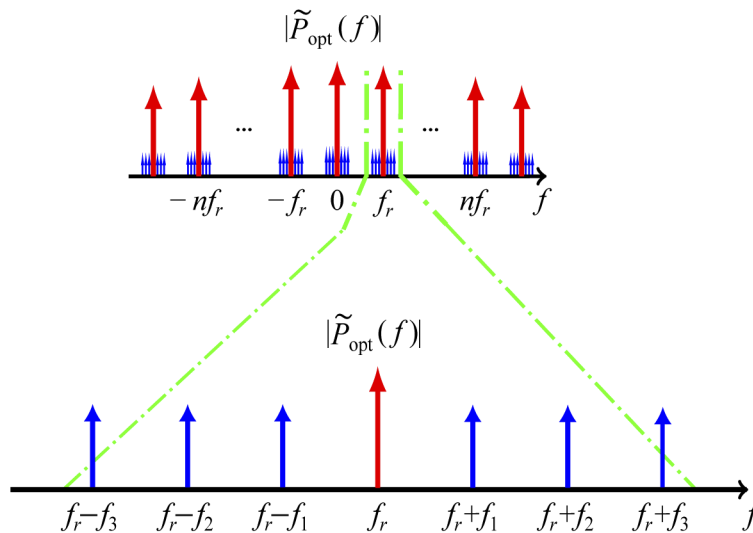


**Fig. 6.** Expanded view of the spectrum of the modulated optical intensity profile. Red arrows show comb lines at harmonics of the repetition frequency. Blue arrows show the comb lines at modulation frequencies ( $nf_r \pm f_1$ ,  $nf_r \pm f_2$ , and  $nf_r \pm f_3$ ) for each comb line where  $n$  is the comb line number. In the expanded view, we show comb lines for  $n = 1$ .

we show the fundamental and modulation frequency components for the first comb line ( $n = 1$ ). Associated with each comb line is a fundamental power  $S_n = S(nf_r)$ , as well as power in each of the modulated components.

Figure 7 shows the power spectrum of the modulated photocurrent. There is a set of comb lines, which are indicated by black arrows. Each comb line is surrounded by lines at the modulation frequencies  $nf_r \pm f_1$ ,  $nf_r \pm f_2$ , and  $nf_r \pm f_3$ , which are shown with blue arrows, lines

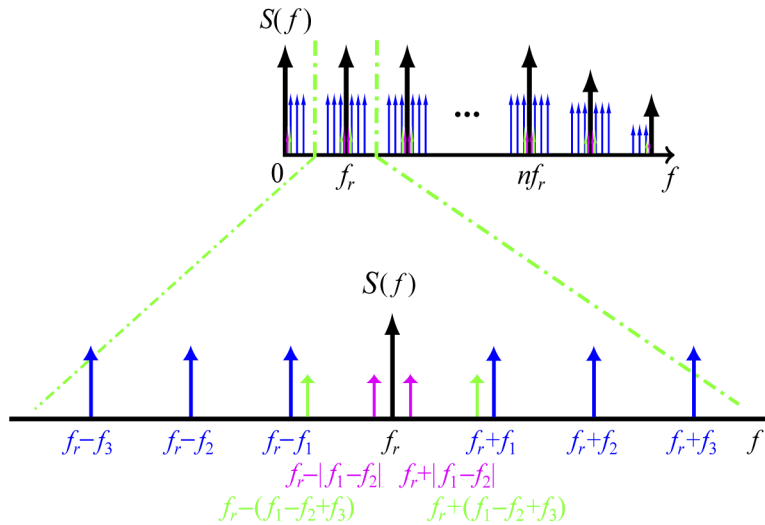


**Fig. 7.** Expanded view of the power spectrum of the modulated photocurrent. Black arrows show comb lines at the harmonics of the fundamental frequency. Blue arrows show comb lines at modulated frequencies ( $nf_r \pm f_1$ ,  $nf_r \pm f_2$ , and  $nf_r \pm f_3$ ) for each comb line, where  $n$  is the comb line number. Magenta arrows show  $\text{IMD}2_n$  lines at  $nf_r \pm (f_1 - f_2)$ . Green arrows show  $\text{IMD}3_n$  lines at  $nf_r \pm (f_1 - f_2 + f_3)$ . In the expanded view, we show comb lines for  $n = 1$ .

at the  $\text{IMD}2_n$  frequencies  $nf_r \pm (f_1 - f_2)$ , which are shown with magenta arrows, and lines at the  $\text{IMD}3_n$  frequencies  $nf_r \pm (f_1 - f_2 + f_3)$ , which are shown with green arrows. In this figure, we show the fundamental frequency, the modulated frequency components, and the additional  $\text{IMD}2_n$  and  $\text{IMD}3_n$  components for the first comb line. In this work, we focused on the  $\text{IMD}2_n$  power at the modulated frequency  $nf_r + (f_1 - f_2)$  and the  $\text{IMD}3_n$  power at the modulated frequency  $nf_r + (f_1 - f_2 + f_3)$ . These are the frequency combinations closest to the fundamental frequency.

## 5. Simulation results for the MUTC PD

We calculate the nonlinearity as a function of the average input optical power  $P_{\text{opt}}(t)$ , given in Eq. (6), for modulation depths  $m = 4\%$  and  $m = 8\%$ . For pulsed inputs, we first calculate the impulse response of the PD for different input optical pulse energies, and we then combine the electrical pulse in the time domain, given by Eq. (7), taking into account the gap of 20 ns between the pulses, to obtain the total electrical response  $P_e(t)$  over a 2- $\mu\text{s}$ -long modulation time. We next calculate the Fourier transform of  $P_e(t)$  in order to determine the harmonic powers of the photocurrent with different choices of the amplitude  $A$ . Using the results, along with Eq. (2), we calculate the nonlinear distortion of a pulsed input both with and without bleaching. The principal effect of bleaching is to lower the responsivity of the PD so that fewer electrons are produced. The lower responsivity decreases the power at the fundamental frequencies  $S_n$ , but also decreases the space charge and hence the nonlinearity, particularly at high frequencies.

Figure 8 compares  $\text{OIP}2_n$  and  $\text{OIP}3_n$  for the MUTC PD with modulation depths  $m = 4\%$  and  $m = 8\%$  when bleaching is included as a function of both comb line frequency and number. As can be seen in Fig. 8,  $\text{OIP}2_n$  and  $\text{OIP}3_n$  are both slightly higher for modulation depth  $m = 4\%$  than for modulation depth  $m = 8\%$ . However, this difference is negligibly small. Changing the modulation depth allows us to validate the assumption that we can expand second- and third-order intermodulation distortion powers quadratically and cubically, respectively. We find that this assumption is valid at least up to modulation depth  $m = 8\%$  [2]. All further results will be

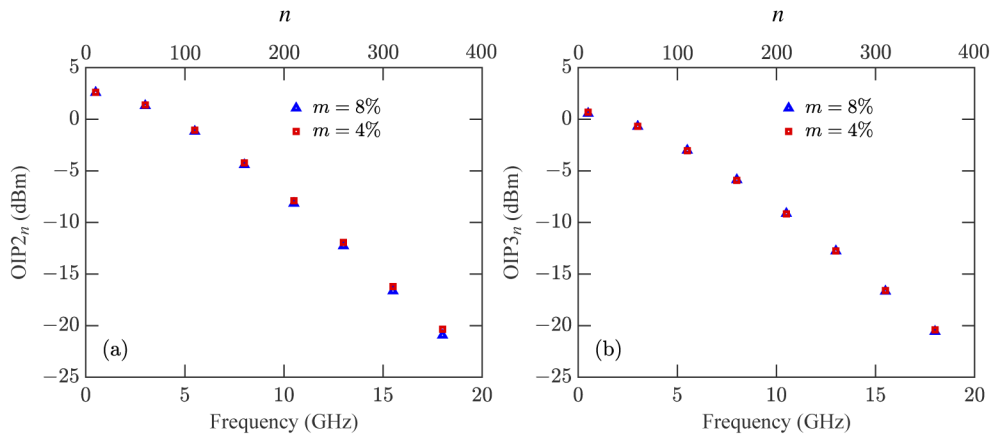
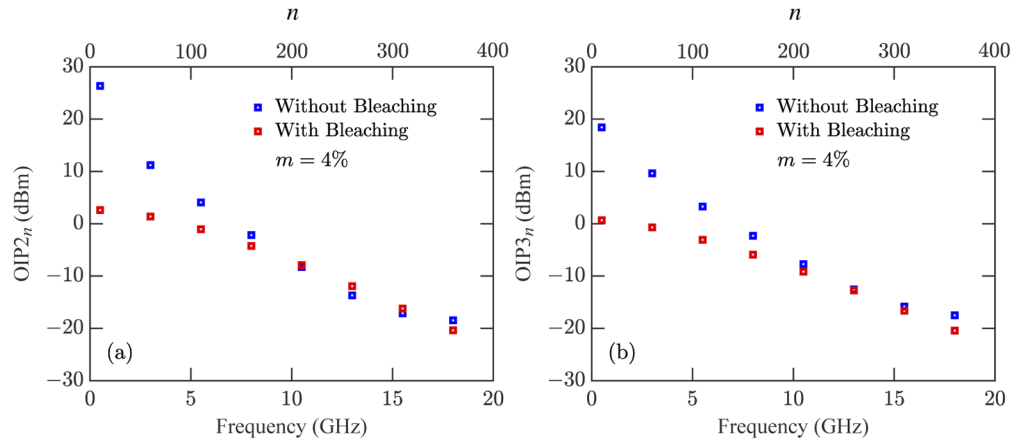


**Fig. 8.** Comparison of (a)  $OIP_{2n}$  and (b)  $OIP_{3n}$  when bleaching is included with  $m = 4\%$  and  $m = 8\%$ .

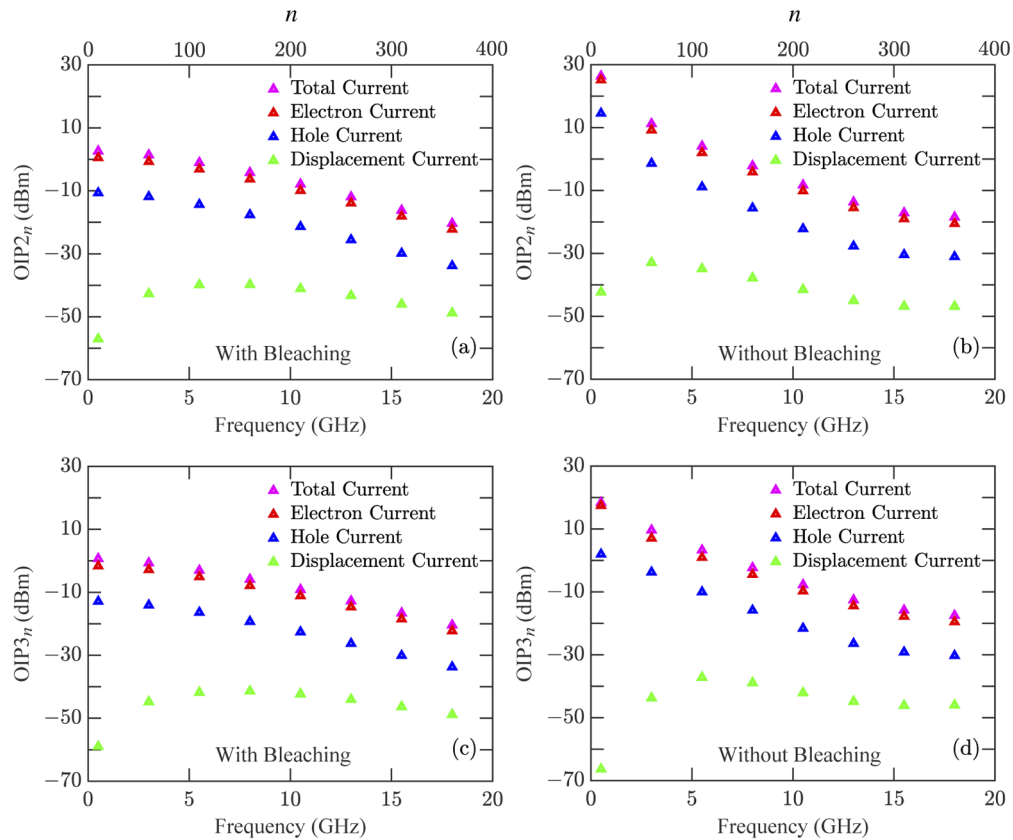
given for modulation depth  $m = 4\%$  since all other results scale appropriately. IMD2 powers are proportional to the square of the modulation depth and IMD3 powers are proportional to the cube of the modulation depth up to  $m = 8\%$ .

Figure 9 shows  $OIP_{2n}$  and  $OIP_{3n}$  as a function of comb line frequency and mode number  $n$  with an average input optical power of 25 mW for the MUTC PD. We show  $OIP_{2n}$  and  $OIP_{3n}$  with and without bleaching. Figure 9(a) shows the intercept point between the  $IMD_{2n}$  power and the fundamental power  $S_n$  in the  $n$ -th comb line, while Fig. 9(b) shows the intercept point between the  $IMD_{3n}$  power and the fundamental power  $S_n$ . These intercept points occur at a lower power when bleaching is included than when it is not. The gap is larger for low comb line numbers. The intercept point decreases both with and without bleaching when  $n$  increases, but this decrease is noticeably slower when bleaching is included so that the intercepts cross and diverge again when  $n$  is large. The falloff of  $OIP_{2n}$  and  $OIP_{3n}$  occurs because the amplitude of the power in the frequency domain decreases as frequency increases. The reason that  $OIP_{2n}$  and  $OIP_{3n}$  are lower when bleaching is included is because bleaching reduces the output power due to the reduction in the responsivity. The behavior of  $OIP_{2n}$  and  $OIP_{3n}$  as a function of comb line frequency is defined by the pattern of the impulse response with and without bleaching in the frequency domain. While the impact of bleaching is to lower the responsivity, which decreases the output power, it also lowers the space charge, which increases the PD bandwidth. As a result we observe that the decrease in  $OIP_{2n}$  and  $OIP_{3n}$  due to bleaching is large at low frequencies, and becomes almost negligible at 15 GHz. It increases again at frequencies beyond 15 GHz where the output power has decreased significantly. Figure 10 shows the separate contribution of the electron current, hole current, and displacement current, as well as the total current as a function of comb line frequency to  $OIP_{2n}$  and  $OIP_{3n}$ . We show results with and without bleaching. Figure 10 shows that displacement current does not contribute significantly to either  $OIP_{2n}$  or  $OIP_{3n}$ . In this figure, we show that the electron current contributes almost 10 dBm more than hole current to  $OIP_{2n}$  and  $OIP_{3n}$ , both with and without bleaching. In MUTC PDs, the electrons are major carriers and holes contribute less to the total current than electrons [15]. The relatively small displacement current demonstrates that the change in time of the electric field contributes negligibly to the total current.

Figure 11 shows the fundamental power  $S_n$ , the  $IMD_{2n}$  power, and the  $IMD_{3n}$  power for  $n = 20$  ( $nf_r = 1$  GHz) and  $n = 200$  ( $nf_r = 10$  GHz). In Fig. 11, the dotted curves show the harmonic powers when bleaching is not included, and the solid curves show the harmonic powers when bleaching is included. In Fig. 2, we showed that the decrease in responsivity due to bleaching



**Fig. 9.**  $OIP_{2n}$  and  $OIP_{3n}$  as a function of comb line frequency and number with an average input optical power of 25 mW. (a)  $OIP_{2n}$ ; (b)  $OIP_{3n}$ .



**Fig. 10.** Contribution of different current components to  $OIP_{2n}$  and  $OIP_{3n}$  as a function of comb line frequency and number. The magenta, red, blue, and green curves show the contributions of the total, electron, hole, and displacement currents, respectively. (a)  $OIP_{2n}$  with bleaching, (b)  $OIP_{2n}$  without bleaching, (c)  $OIP_{3n}$  with bleaching, (d)  $OIP_{3n}$  without bleaching.

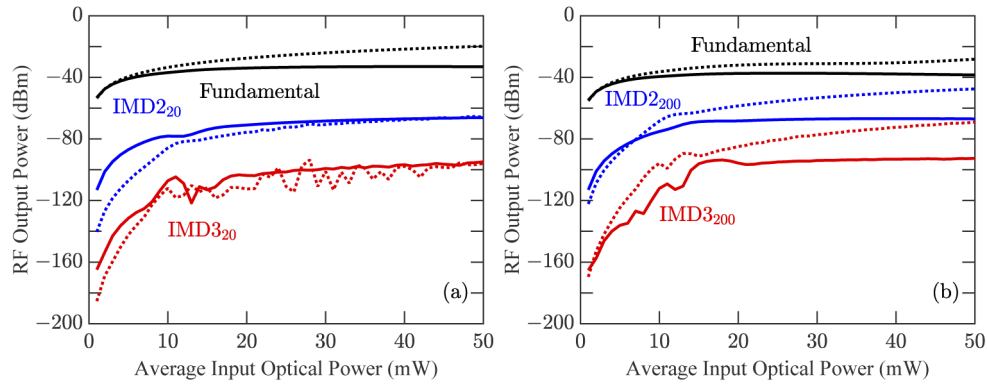


**Fig. 11.** Power at the fundamental frequency ( $nf_r$ ), the  $IMD_{2n}$  power at the modulated frequency  $nf_r + (f_1 - f_2)$ , and the  $IMD_{3n}$  power at the modulated frequency  $nf_r + (f_1 - f_2 + f_3)$ . Solid lines show results with bleaching; dotted lines show results without bleaching: (a)  $n = 20$  ( $nf_r = 1$  GHz), (b)  $n = 200$  ( $nf_r = 10$  GHz).

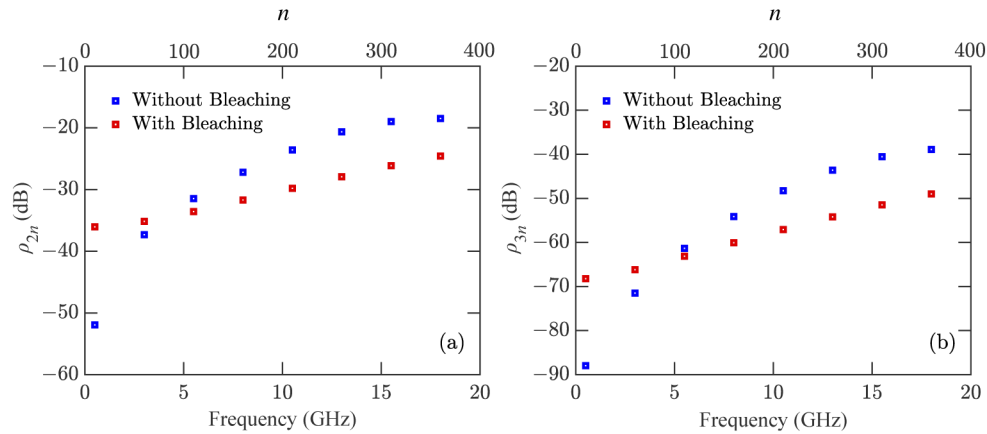


**Fig. 12.** Distortion to signal ratios as a function of comb line frequency and number with and without bleaching for: (a)  $\rho_{2n}$ , (b)  $\rho_{3n}$ .

becomes greater as the optical power increases. That leads to a decrease in the fundamental power, which becomes more pronounced as the frequency increases. For lower frequency comb lines,  $n \lesssim 50$ , we find that the  $IMD_{2n}$  and  $IMD_{3n}$  powers are higher when bleaching is included, but for higher frequency comb lines, the  $IMD_{2n}$  and  $IMD_{3n}$  powers are higher when bleaching is not included.

Figure 12 shows the distortion-to-signal ratios  $\rho_{2n} = IMD_{2n}/S_n$  and  $\rho_{3n} = IMD_{3n}/S_n$  as a function of comb line frequency. Figure 12 shows that the ratios  $\rho_{2n}$  and  $\rho_{3n}$  increase as the comb line number increases, so that the impact of nonlinearity increases. The third-order intermodulation products are particularly important because these products can introduce spurious signals that cannot be filtered out from the fundamental response. This is important for microwave photonics applications where these spurious signals would appear as false signals of interest [4]. We also find that the curves for  $\rho_{2n}$  and  $\rho_{3n}$  cross over at 5 GHz, so that beyond 5 GHz  $\rho_{2n}$  and  $\rho_{3n}$  are smaller with bleaching than they are without bleaching. While the reduction in responsivity due to bleaching leads to a decrease in the signal components,  $S_n$ , the accompanying

reduction in space charge and hence  $\text{IMD}_{2n}$  and  $\text{IMD}_{3n}$  more than compensates for the decrease in  $S_n$ .

## 6. Conclusion

We have developed an empirical model of bleaching based on experimental data that were collected at the Naval Research Laboratory and we have incorporated this model into the 1-D drift-diffusion equations. We then used this model to study the impact of nonlinearity in an MUTC PD on electro-optic frequency combs. The principal effect of bleaching is to lower the responsivity and hence the space charge, which decreases the impact of nonlinearity at high frequencies.

We use the three-tone modulation technique to calculate  $\text{IMD}_2$  and  $\text{IMD}_3$  when the PD operates with a pulsed input. We calculated  $\text{OIP}_2$  and  $\text{OIP}_3$  to characterize  $\text{IMD}_2$  and  $\text{IMD}_3$ . When the input to the PD is a train of RF-modulated optical pulses, the output of the PD is a modulated electrical pulse train that corresponds to a set of frequency comb lines in the frequency domain. By contrast to a CW input for which there is one  $\text{IMD}_2$  and one  $\text{IMD}_3$ , each comb line has its own  $\text{IMD}_2$  and  $\text{IMD}_3$ . We determined the behavior of  $\text{IMD}_{2n}$ ,  $\text{IMD}_{3n}$ ,  $\text{OIP}_{2n}$ , and  $\text{OIP}_{3n}$  for each comb line  $n$  with and without bleaching. We found that  $\text{OIP}_{2n}$  and  $\text{OIP}_{3n}$  occur at a lower power when bleaching is included than when it is not. The gap is larger for low comb line numbers. The intercept point decreases both with and without bleaching when  $n$  increases, but this decrease is noticeably slower when bleaching is included so that the intercepts converge when  $n$  is large.

We determined the contribution of electron current, hole current, and displacement current to  $\text{OIP}_{2n}$  and  $\text{OIP}_{3n}$ . We showed that displacement current does not play a major role both in  $\text{OIP}_{2n}$  and  $\text{OIP}_{3n}$ , and electron current contributes almost 10 dBm more than hole current in  $\text{OIP}_{2n}$  and  $\text{OIP}_{3n}$  both with and without bleaching. In MUTC PDs electrons are major carriers, and holes contribute less to the total current than electrons.

We calculated distortion-to-signal ratios  $\rho_{2n}$  and  $\rho_{3n}$  as a function of comb line frequency with and without bleaching. We found that these ratios increase as the comb line number increases, so that the fraction of each comb line power in  $\text{IMD}_{2n}$  and  $\text{IMD}_{3n}$  increases.

The decrease in the electron number due to bleaching becomes more pronounced when the input power increases, as a result of which the fundamental comb powers  $S_n$  and the intermodulation products eventually saturate as the input optical power increases. Simultaneously, as previously noted, the smaller number of electrons in the device lowers the nonlinearity due to space charge effects. We find that the  $\text{OIP}_{2n}$  and  $\text{OIP}_{3n}$  powers decrease as  $n$  increases whether or not bleaching is included. However, the impact of bleaching is strongest at lower comb line frequencies, almost disappears at comb line frequencies between 10 GHz and 15 GHz, and reappears again at comb line frequencies beyond 15 GHz.

As a consequence, the impact of bleaching on the ratios  $\rho_{2n}$  and  $\rho_{3n}$  is complex and not always detrimental. When  $n \lesssim 100$  ( $\lesssim 5$  GHz), we find that the ratio is higher when bleaching is included. On the other hand, when  $n \gtrsim 100$  ( $\gtrsim 5$  GHz), the ratio is lower when bleaching is included, so that bleaching actually improves this ratio at comb line frequencies beyond 5 GHz.

**Funding.** U.S. Naval Research Laboratory (N00173-15-1-G905).

**Acknowledgment.** A portion of our computational work was carried out at the UMBC High Performance Computing Facility (<https://hpcf.umbc.edu>).

**Disclosures.** The authors declare no conflicts of interest.

## References

1. S. E. Jamali Mahabadi, T. F. Carruthers, C. R. Menyuk, J. D. McKinney, and K. J. Williams, "Impact on frequency combs of nonlinearity including bleaching in  $p-i-n$  photodetectors," in *IEEE Photonics Society Summer Topicals Meeting Series* (IEEE, 2020), pp. 1–2.
2. S. E. Jamali Mahabadi, T. F. Carruthers, C. R. Menyuk, M. N. Hutchinson, J. D. McKinney, and K. J. Williams, "Impact of nonlinearity on RF-modulated frequency combs with different modulation depths in an MUTC photodetector," in *IEEE International Topical Meeting on Microwave Photonics* (IEEE, 2019), pp. 1–4.
3. S. E. Jamali Mahabadi, T. F. Carruthers, C. R. Menyuk, M. N. Hutchinson, J. D. McKinney, and K. J. Williams, "Impact of nonlinearity in an MUTC photodetector on an RF-modulated frequency comb," in *IEEE Photonics Conference* (IEEE, 2019), pp. 1–2.
4. S. E. Jamali Mahabadi, T. F. Carruthers, C. R. Menyuk, J. D. McKinney, and K. J. Williams, "Comparison of the impact of nonlinearity in a  $p-i-n$  and an MUTC photodetector on electro-optic frequency combs," *Opt. Lett.* **46**(4), 813–816 (2021).
5. V. J. Urick, K. J. Williams, and J. D. McKinney, *Fundamentals of Microwave Photonics* (Wiley, 2015), pp. 407–415.
6. M. Fortier, M. S. Kirchner, F. Quinlan, J. Taylor, J. C. Bergquist, T. Rosenband, N. Lemke, A. Ludlow, Y. Jiang, C. W. Oates, and S. A. Diddams, "Generation of ultrastable microwaves via optical frequency division," *Nat. Photonics* **5**(7), 425–429 (2011).
7. J. Millo, R. Boudot, M. Lours, P. Y. Bourgeois, A. N. Luiten, Y. Le Coq, Y. Kersale, and G. Santarelli, "Ultra-low-noise microwave extraction from fiber-based optical frequency comb," *Opt. Lett.* **34**(23), 3707–3709 (2009).
8. S. R. Harmon and J. D. McKinney, "Broadband RF disambiguation in subsampled analog optical links via intentionally-introduced sampling jitter," *Opt. Express* **22**(20), 23928–23937 (2014).
9. S. A. Diddams, "The evolving optical frequency comb," *J. Opt. Soc. Am. B* **27**(11), B51–B62 (2010).
10. J. D. McKinney and K. J. Williams, "Sampled analog optical links," *IEEE Trans. Microwave Theory Tech.* **57**(8), 2093–2099 (2009).
11. P. W. Juodawlkis, F. J. O'Donnell, J. J. Hargreaves, D. C. Oakley, A. Napoleone, S. H. Groves, L. J. Molvar, K. M. Mahoney, L. J. Missaggia, J. P. Donnelly, R. C. Williamson, and J. C. Twichell, "Absorption saturation nonlinearity in InGaAs/InP  $p-i-n$  photodiodes 2," in *15th Annual Meeting of the IEEE Lasers and Electro Optics Society* (IEEE, 2002), pp. 426–427.
12. Y. Hu, C. R. Menyuk, X. Xie, M. N. Hutchinson, V. J. Urick, J. C. Campbell, and K. J. Williams, "Computational study of amplitude-to-phase conversion in a modified untraveling carrier photodetector," *IEEE Photonics J.* **9**(2), 1–11 (2017).
13. Z. Li, H. Pan, H. Chen, A. Beling, and J. C. Campbell, "High-saturation-current modified uni-traveling-carrier photodiode with cliff layer," *IEEE J. Quantum Electron.* **46**(5), 626–632 (2010).
14. A. E. Siegman, *Lasers* (University Science Books, 1986).
15. S. E. Jamali Mahabadi, S. Wang, T. F. Carruthers, C. R. Menyuk, F. J. Quinlan, M. N. Hutchinson, J. D. McKinney, and K. J. Williams, "Calculation of the impulse response and phase noise of a high-current photodetector using the drift-diffusion equations," *Opt. Express* **27**(3), 3717–3730 (2019).
16. D. M. Pozar, *Microwave Engineering* (Wiley, 2009).
17. I. P. Kaminow, T. Li, and A. E. Willner, *Optical Fiber Telecommunications Volume A: Components and Subsystems* (Academic, 2008).
18. M. N. Draa, A. S. Hastings, and K. J. Williams, "Comparison of photodiode nonlinearity measurement systems," *Opt. Express* **19**(13), 12635–12645 (2011).
19. Y. Hu, "Modeling Nonlinearity and Noise in High-Current Photodetectors," in Ph.D. Dissertation, University of Maryland, Baltimore County, Maryland, USA, 2017.
20. F. Quinlan, T. M. Fortier, H. Jiang, and S. A. Diddams, "Analysis of shot noise in the detection of ultrashort optical pulse trains," *J. Opt. Soc. Am. B* **30**(6), 1775–1785 (2013).